Key Points:
- Fe$_3$C decomposes into a mixture of solid Fe$_7$C$_3$ and hcp-Fe above 145 GPa prior to melting
- Fe$_3$C liquidus is ~5100 K at 185 GPa, which is ~500 K higher than Fe melting point by Anzellini et al.
- Fe$_7$C$_3$ may solidify out of the early outer core to become a component of the innermost inner core

Phase relations of Fe$_3$C and Fe$_7$C$_3$ up to 185 GPa and 5200 K: Implication for the stability of iron carbide in the Earth's core

Jin Liu[1,2] (iD), Jung-Fu Lin[1,3] (iD), Vitali B. Prakapenka[4] (iD), Clemens Prescher[4] (iD), and Takashi Yoshino[5] (iD)

[1]Department of Geological Sciences, Jackson School of Geosciences, University of Texas at Austin, Austin, Texas, USA, [2]Now at Department of Geological Sciences, Stanford University, Stanford, California, USA, [3]Center for High Pressure Science and Technology Advanced Research, Shanghai, China, [4]Consortium for Advanced Radiation Sources, University of Chicago, Chicago, Illinois, USA, [5]Institute for Planetary Materials, Okayama University, Okayama, Japan

Abstract We have investigated phase relations and melting behavior of Fe$_3$C and Fe$_7$C$_3$ using X-ray diffraction in a laser-heated diamond cell up to 185 GPa and 5200 K. Our results show that the starting Fe$_3$C sample decomposes into a mixture of solid orthorhombic Fe$_7$C$_3$ and hcp-Fe at above 145 GPa upon laser heating and then transforms into Fe-C liquid and solid Fe$_7$C$_3$ at temperatures above 3400 K. Using the intensity of the diffuse scattering as a primary criteria for detecting melting, the experimentally derived liquidus for a bulk composition of Fe$_3$C fitted with the Simon-Glatzel equation is $T_m(K) = 1800 \times [1 + (P_m - 5.7)/15.10 \pm 2.55]^{1/2.41 \pm 0.17}$ at 24–185 GPa, which is ~500 K higher than the melting curve of iron reported by Anzellini et al. (2013) at Earth's core pressures. The higher melting point and relative stability of Fe$_7$C$_3$ in Fe-rich Fe-C system at Earth's core conditions indicate that Fe$_7$C$_3$ could solidify out of the early Earth's molten core to become a constituent of the innermost inner core.

1. Introduction

The Earth's core is primarily composed of Fe-Ni alloy with approximately 5–10 wt % light element(s), such as C, O, Si, and S (see *Li and Fei* [2014] for a recent review). Carbon has been commonly considered as a potential major light element as it is the fourth most abundant element in the solar system and its abundance reaches 3.2 wt % in the carbonaceous chondrites-Ivuna (CI). A number of iron carbide phases (e.g., Fe-rich Fe-C alloys, Fe$_3$C, Fe$_7$C$_3$, or Fe$_2$C) have been proposed to be the carbon-bearing host phase in the core [e.g., *Wood*, 1993; *Dasgupta et al.*, 2009; *Lord et al.*, 2009; *Nakajima et al.*, 2009; *Tateno et al.*, 2010; *Bazhanova et al.*, 2012; *Fei and Brosh*, 2014; *Liu et al.*, 2016a]. Studies of their high-pressure-temperature (*P-T*) properties including crystal structures and melting curves are thus essential to understanding Earth's accretion and early differentiation as well as the deep-carbon cycle.

Based on previous high-pressure studies, intermediate Fe-C compounds such as Fe$_3$C and Fe$_7$C$_3$ have been considered as the most likely candidates for the carbon-bearing phase in the core, partly due to the limited solubility of carbon in hcp-Fe [e.g., *Wood*, 1993; *Gao et al.*, 2008; *Lord et al.*, 2009; *Nakajima et al.*, 2009; *Chen et al.*, 2014]. Using a thermodynamically calculated phase diagram of the Fe-C system up to core pressures, *Wood* [1993] proposed that Fe$_3$C could be a primary component in the inner core, which was experimentally found to be stable up to 187 GPa at 300 K and 73 GPa at ~1500 K, respectively, in X-ray diffraction studies [*Scott et al.*, 2001; *Li et al.*, 2002; *Sata et al.*, 2010; *Litasov et al.*, 2013]. Fe$_3$C undergoes magnetic transitions at high pressures that can further affect our understanding of its properties as a carbon host [*Lin et al.*, 2004; *Duman et al.*, 2005; *Gao et al.*, 2008; *Prescher et al.*, 2012]. Fe$_3$C was recently observed to melt incongruently producing liquid Fe-C alloy and a more carbon-rich carbide, Fe$_7$C$_3$, in temperature quenching above 5–10 GPa in the multianvil press experiments [*Dasgupta et al.*, 2009; *Nakajima et al.*, 2009; *Fei and Brosh*, 2014]. Most of recent experimental and theoretical studies on the Fe-C system thus indicated that Fe$_7$C$_3$ could become more stable than Fe$_3$C as a carbon-bearing phase in the core [e.g., *Lord et al.*, 2009; *Mookherjee et al.*, 2011; *Nakajima et al.*, 2011; *Chen et al.*, 2012]. The high Poisson's ratio of Fe$_7$C$_3$ at high pressures matches that of the preliminary reference Earth model (PREM) for the inner core, further supporting its potential presence in the region [*Chen et al.*, 2014; *Prescher et al.*, 2015]. However, recent sound velocity measurements of Fe-C system have showed that carbon can be ruled out as a major light element due to its velocity mismatch with the outer core [*Nakajima et al.*, 2015]. On the basis of melting temperatures of

the Fe-C eutectic, Fe_3C, and Fe_7C_3 at moderate pressures up to 70 GPa, *Lord et al.* [2009] further argued that Fe_7C_3 would replace Fe_3C to form a eutectic relation with Fe approximately above 130 GPa. The observation of plateaus in the temperature-laser power profile was used as the principal melting criterion by *Lord et al.* [2009]. In addition, the motion of the sample surface, the texture of quenched samples, and the plateau in the temperature-emissivity profile have been used as the melting indicators in previous studies [e.g., *Williams et al.*, 1987; *Boehler et al.*, 1990; *Boehler*, 1993; *Campbell*, 2008; *Lord et al.*, 2009]. The melting criteria in these previous studies are secondary diagnostics for melting and have been highly debated [e.g., *Shen et al.*, 2004; *Anzellini et al.*, 2013]. Furthermore, most of these previous works were limited to below 100 GPa, which is substantially lower than the inner core *P-T* conditions. Therefore, in situ high *P-T* studies on the Fe-rich portion of the Fe-C system at pressures above 135 GPa, coupled with a reliable probe for detecting melting, are critically needed to assess the presence of iron carbide in the core.

In this study, we have investigated the phase stability and melting behavior of Fe_3C and Fe_7C_3 using synchrotron X-ray diffraction (XRD) techniques combined with the double-sided burst laser heating in a diamond anvil cell (DAC). The integrated intensity of diffuse scattering signals from the liquid in the measured XRD patterns was used as the primary diagnostic for melting and the amount of melt in the present work (Figure S1 in the supporting information) [*Shen et al.*, 2004; *Anzellini et al.*, 2013]. Our results show that Fe_3C incongruently melts into liquid Fe-C alloy and solid Fe_7C_3 below 145 GPa, while at higher pressures it decomposes into a mixture of solid Fe_7C_3 and hcp-Fe prior to melting into Fe_7C_3 and Fe-C liquid. These results are integrated with previous thermodynamically modeled results for the system and melting curves of hcp-Fe to better understanding the phase relations of the Fe-rich portion of the Fe-C system under *P-T* conditions relevant to the Earth's core.

2. Experiments

Polycrystalline Fe_3C sample was synthesized from a mixture of iron and graphite powder (>99.99% purity) with an atomic ratio of 3:1. The Fe-C mixture was then packed in an MgO capsule and equilibrated at 1 GPa and 1373 K for 18 h using the end-loaded piston cylinder apparatus at the Institute for Study of the Earth's Interior, Okayama University at Misasa. The synthesized sample pellet was recovered at ambient conditions and analyzed using XRD and electronic microprobe analyses which confirmed the polycrystalline single phase of Fe_3C in the orthorhombic structure (space group: *Pnma*). Material with an average grain size less than 1 μm was then removed from the pellet and slightly compressed between two diamond anvils with a culet of 600 μm to make thin discs of 3–7 μm thick. These sample discs of the polycrystalline Fe_3C were loaded into diamond anvil cells (DACs) with a pair of anvils with the culet size varying between 400 μm flat and 100–300 μm beveled. Commercial KCl (>99.997%, Alfa Aesar) was used as the pressure-transmitting medium and thermal insulation from the diamond surfaces and the rhenium gasket. KCl was dried at 800 K in an oven prior to loading and was then compressed to make KCl discs of 3–8 μm thick using a DAC. A Re gasket of 250 μm thick was preindented to 25 GPa, and a hole varying between 60 and 250 μm in diameter was drilled in the center of the preindention to make a sample chamber. The KCl layers were prepared to be as even and thick as possible so that the Fe_3C sample could be well insulated for stable heating especially at extremely high temperatures above 1 Mbar for observation of the occurrence of the X-ray diffuse scattering signals in the laser-heating experiments. Each DAC loaded with the Fe_3C and KCl assemblage in the sample chamber was vacuumed for 1 h before the sample chamber was sealed by closing the DAC using the high-pressure gas loader in the Mineral Physics Laboratory of the University of Texas at Austin.

The XRD experiments in a laser-heated DAC were conducted at the GeoSoilEnviroConsortium for Advanced Radiation Sources (GSECARS) of Advanced Photon Source (APS), Argonne National Laboratory using a burst-heating technique [*Prakapenka et al.*, 2008]. Laser-heating XRD experiments at each *P-T* were completed in 1–2 s, by synchronizing the operation of laser shutter, temperature measurements, and the collection of in situ X-ray diffraction. Temperatures and temperature uncertainties were determined from ~10 thermal radiation spectra from both sides of the laser-heating system, which were collected over the course of each heating experiment (1–2 s). The thermal radiation spectra were fitted to the Planck radiation function assuming the graybody approximation [*Prakapenka et al.*, 2008]. The uncertainty in temperature is about 50–200 K estimated from both heating sides. The advent of diffuse scattering ring in the XRD patterns provide robust evidence for the presence of melting in the sample chamber [*Shen et al.*, 2004; *Anzellini et al.*, 2013; *Liu et al.*,
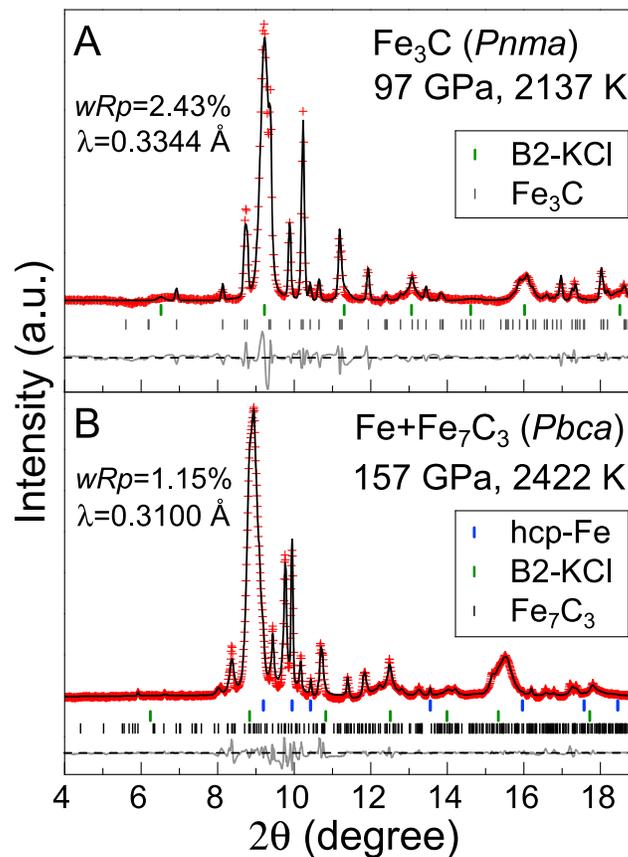
Figure 1. Representative LeBail fits of X-ray diffraction spectra with Fe_3C as the starting sample at high pressure and temperature. (a) LeBail fit revealed phases of orthorhombic Fe_3C and B2-KCl at 97 GPa and 2137 (±52) K. (b) LeBail fit revealed phases of orthorhombic Fe_7C_3 (o-Fe_7C_3), hcp-Fe, and B2-KCl at 157 GPa and 2422 (±65) K. Pluses: measured powder diffraction patterns after background subtraction; black solid curves: refined profiles; gray solid curves: residue between the observation and the refinement; vertical ticks: B2-KCl (olive), hcp-Fe (blue), o-Fe_7C_3 (black), and Fe_3C (gray). The crystal structure of o-Fe_7C_3 used in the LeBail fit was based on the *Pbca* space group model reported by *Prescher et al.* [2015]. The weighted *R* factor (*wRp*) after background subtraction in the plot was taken from the refinement using the GSAS software package. The wavelength of the incident X-ray beam was 0.3100 Å and 0.3344 Å for 157 and 97 GPa, respectively.

2016b]. The burst-heating technique minimizes the sample's exposure to the laser beam, which can prevent chemical reactivity and diffusion, therefore, enable accurate measurement of melting curves and phase changes and reach higher temperatures compared to laser-heating experiments with long laser exposure. X-ray diffraction patterns of the sample were collected by a MAR CCD detector before, during, and after laser heating and were integrated and analyzed using DIOPTAS [*Prescher and Prakapenka*, 2015] and GSAS software packages [*Larson and Dreele*, 1994; *Toby*, 2001]. The tilting and rotation of the detector relative to the incident X-ray beam and the sample-to-detector distance were calibrated by diffraction of lanthanum hexaboride (LaB6) powder at ambient conditions. Because the thermal equation of state (EoS) for Fe_7C_3 in the orthorhombic structure has not been determined, pressures were obtained from the measured lattice parameters of KCl using the EoS for the B2 structure at 300 K [*Dewaele et al.*, 2012]. When possible, we obtained pressures using the thermal EoS for Fe_3C [*Nakajima et al.*, 2011] and hcp-Fe [*Fei et al.*, 2016], which were found to be comparable to pressures within ±2–4 GPa obtained from the measured lattice parameters of B2-KCl using its EoS at 300 K. Because the transparent

pressure medium and thermal insulator do not act as a laser absorber, the 300 K EoS has been found to give similar pressures to that of the hot sample in cases where the thermal equation of state of the sample was known [*Campbell et al.*, 2007]. The reported pressures from KCl thus represent a minimum estimate without correction for thermal pressure and may underestimate the pressure by a few GPa [*Anzellini et al.*, 2013].

3. Results and Discussion

X-ray diffraction patterns of the samples were collected at high pressures up to 185 GPa between 300 K and 5200 K (Figures S1–S2 and Table S1). All diffraction peaks of the starting materials can be well indexed with an orthorhombic structure of Fe_3C (space group: *Pnma*) up to 133 GPa and 3200 K (Figures 1a and S3). At 157 GPa and 2422 K, several key diffraction peaks could not be indexed by the unit cell of Fe_3C but match the diffraction peaks of hcp-Fe, which were not observed in the diffraction pattern before heating at 157 GPa (Figure 1b). The remaining diffraction peaks at 157 GPa can be better indexed with an orthorhombic structure of Fe_7C_3 (space group: *Pbca*) using the reported structural model by *Prescher et al.* [2015] (Figure 1b). The

Figure 2. Observed phases in the Fe-rich Fe-C system with Fe$_3$C as the starting sample at high pressure and temperature. Experimentally observed phases are displayed as squares (Fe$_3$C), blue diamonds (Fe$_7$C$_3$ + liquid), gray diamonds (Fe$_7$C$_3$ + Fe), and circles (liquid). Dashed lines represent schematic boundaries between these phases. Insert: a representative sample after being laser heated at 117 GPa and 4938 ($\pm$53) K (A), 134 GPa and 4284 ($\pm$184) K (B), and 141 GPa and 5004 ($\pm$147) K (C), respectively. Re was the gasket, and KCl was used as the pressure-transmitting medium in this study (transparent area in the inset).

results suggest that the Fe$_3$C phase decomposes into hcp-Fe and orthorhombic Fe$_7$C$_3$ at pressures above 145 GPa upon laser heating (Figure 2).

Upon increasing temperatures, e.g., at 76 GPa and above 2600 K, diffuse scattering rings were observed in the diffraction patterns where the strongest intensities of X-ray reflections from Fe$_3$C started to diminish (Figures 3 and S1). The diffraction lines, coexisting with the diffuse scattering rings, could be well indexed with Fe$_7$C$_3$ at 76 GPa and ~2800 K, suggesting that Fe$_3$C melts incongruently at this pressure. The observed melting relation is consistent with the results of multianvil experiments at pressures between 5 and 20 and thermodynamic calculations [*Nakajima et al.*, 2009; *Fei and Brosh*, 2014]. After the laser was turned off, the sharp diffraction peaks from Fe$_7$C$_3$ and Fe replaced the diffuse scattering rings. The validity of the diffuse scattering rings corresponding to the Fe-rich liquid was confirmed by the first sharp peak position of the liquid which was close to that of Fe liquid at high pressures [*Shen et al.*, 2004]. The observation of the diffuse scattering ring during laser heating was then used as the primary indication for the presence of melt in the sample, in accordance with previous high-pressure melting studies on Fe and Fe-Fe$_3$C [e.g., *Shen et al.*, 2004; *Liu et al.*, 2016b]. Furthermore, the integrated diffuse scattering signals from the liquid were calculated from their integrated intensity after subtraction of diffraction peaks from solids as well as the background (Figure 3b). The integrated intensity was then normalized using the integrated intensity at the highest temperatures of the heating experiments where the intensity appeared to remain constant with increasing temperature (Figure 3c); such an observation was taken as the sample being fully melted. The normalized intensity of the diffuse scattering signals from the liquid after proper background removal increases with increasing temperature before it flattens out altogether with the complete disappearance of the reflections from Fe$_7$C$_3$ (Figure 3). The total intensity of the diffuse scattering signals thus can be used as a reliable means to refer the ratio between the liquid and the relevant solid. At a given pressure of 76 GPa, for example, the initial appearance of the integrated intensity at ~2600 K indicates the starting occurrence of the liquid phase and can thus be used to indicate the solidus temperature ($T_{solidus}$), while the appearance of a plateau in the integrated diffuse signals from the liquid starting at ~3600 K indicates a complete melting of the system above the liquidus ($T_{liquidus}$).

Assuming that the liquid structural factors vary minimally within the explored temperature range at a given pressure in this study, the normalized intensity of diffuse scattering signals from the Fe-rich liquid could primarily reflect the volume fraction of melt (N_{melt}) in the laser-heated area, which can be fitted to an exponential function of the temperature

$$N_{melt} = 1/\left[1 + \exp\left(a_0 + a_1(T - T_{solidus})/(T_{liquidus} - T_{solidus})\right)\right] \quad (1)$$

where a_0 and a_1 are two pressure-dependent constants, and $T_{solidus}$ and $T_{liquidus}$ are the solidus and liquidus of the sample at a given pressure, respectively. The $T_{solidus}$ and $T_{liquidus}$ of the incongruent melting system thus can be distinctly determined by fitting to the normalized intensity of liquid diffuse signal for each heating series (Figure 3). The fitted $T_{solidus}$ of Fe$_3$C at 24 GPa was about 1950 K, agreeing well with *Nakajima et al.* [2009] and *Fei and Brosh* [2014], but lower by 400 K than that reported by *Lord et al.* [2009]. This discrepancy between our study and *Lord et al.* [2009] may be attributed to the use of melting criteria in these studies: the

Figure 3. Representative X-ray diffraction patterns at 76 GPa and high temperatures with Fe_3C as the starting sample. (a) Diffuse scattering signal from the liquid phase. The olive region represents the diffuse signal of the liquid at 4020 K. Diffraction peaks of B2-KCl were labeled as KCl. (b) Integrated XRD signals after diffraction peaks from solids have been masked. The elevation of the profiles at higher temperatures with respect to the profile at 2479 K represents the presence of liquid in the sample at high temperatures. Insert: diffuse signals after the background subtraction using a reference profile at 1441 K where the XRD signals were only from the solid. (c) Normalized liquid diffuse signal ratio as a function of temperature. The flattening of the integrated diffuse signal from the liquid at above ~3600 K was used as an evidence for the complete melting of the system. The diffuse signals were normalized for the derived ratios in the vertical axis using the average value of the plateau as the reference. Red line: polynomial fit to the experimental data. The shadow region represents the solidus and liquidus at ratios of 5% and 95%, respectively, by considering the temperature uncertainty of approximately 5–10% on the experimental data.

$T_{solidus}$ and $T_{liquidus}$ of the incongruent melting of Fe_3C were not separately recognized on the observational basis of the plateaus in the temperature-laser power profile used by *Lord et al.* [2009]. The fitted $T_{liquidus}$ of Fe_3C at 24 GPa was about 2450 K, and the temperature difference (ΔT) between the $T_{solidus}$ and $T_{liquidus}$ of the sample was approximately 500 K, which was about 200–300 K higher than those reported from multianvil experiments using quenched textures as a melting criterion [*Nakajima et al.*, 2009; *Fei and Brosh*, 2014]. The difference in the derived $T_{liquidus}$ of Fe_3C in these studies indicates that these melting criteria remain to be further reconciled in high *P-T* experiments.

The measured solidus and liquidus of the samples as a function of pressure are fitted to the Simon-Glatzel equation, respectively (Figure 4):

$$T_m = T_0[1 + (P_m - P_0)/a]^{1/c} \quad (2)$$

where T_m and P_m are the temperature and pressure of solidus and liquidus, respectively, *a* and *c* are two composition-dependent constants, and T_0 and P_0 are the melting temperature-pressure at the triple point [*Simon and Glatzel*, 1929]. The Kraut-Kennedy equation was not used in this study due to its doubtful applicability to an incongruently melting compound [*Lord et al.*, 2009]. For the $T_{solidus}$ of Fe_3C at 24–145 GPa, the fitted parameters are $a = 43.05$ (± 8.56) GPa and $c = 1.73$ (± 0.21) with a fixed T_0 and P_0 at 1420 K and 0.0001 GPa for the ambient melting temperature of Fe_3C. For the $T_{solidus}$ of Fe_7C_3-Fe at 145–185 GPa, the fitted parameters are $a = 27.99$ (± 0.39) GPa and $c = 4.83$ (± 0.03), and the triple point is estimated to be at $T_0 = 3400$ K and $P_0 = 145$ GPa. For the $T_{liquidus}$
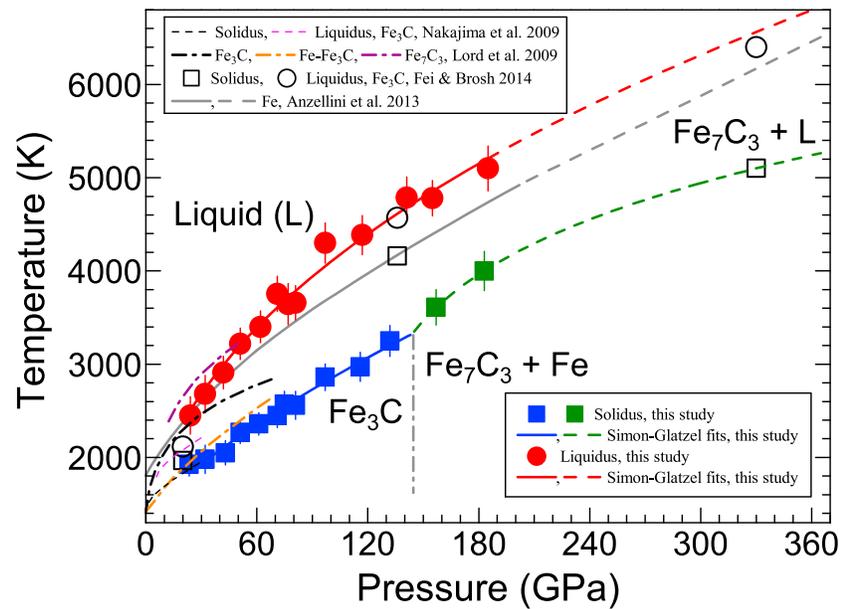
Figure 4. Melting relations of Fe-rich Fe-C phases at high pressure and temperature. Solid squares and circles: solidus and liquidus, respectively (this study); open squares and circles: solidus and liquidus calculated by *Fei and Brosh* [2014]; blue and red solid lines: fits to our experimental data using the Simon-Glatzel equation (this study); red dashed line: extrapolated to the Earth's inner core (this study); gray dash-dotted line: phase boundary between solid Fe_3C and a mixture of solid Fe and Fe_7C_3 phases (this study); olive dashed line: phase boundary between solid Fe and Fe_7C_3 and liquid (this study [*Fei and Brosh*, 2014]); gray solid and dashed lines: experimental and extrapolated melting curve of Fe, respectively [*Anzellini et al.*, 2013]; black and magenta dashed lines: solidus and liquidus of Fe_3C, respectively [*Nakajima et al.*, 2009]; black, orange, and purple dash-dotted lines: the melting temperature of Fe_3C, $Fe-Fe_3C$, and Fe_7C_3, respectively [*Lord et al.*, 2009]. Vertical ticks represent the standard deviation calculated using standard error propagations.

of the sample at 24–185 GPa, the fitted parameters are $a = 15.10$ (± 2.55) GPa and $c = 2.41$ (± 0.17), with the triple point approximately at $T_0 = 1800$ K and $P_0 = 5.7$ GPa from diamond + liquid to Fe_7C_3 + liquid by *Nakajima et al.* [2009]. The present $T_{solidus}$ of Fe_3C was well in line with the multianvil experiments by *Nakajima et al.* [2009] and *Fei and Brosh* [2014]. The melting curve of Fe_3C reported by *Lord et al.* [2009] was located between the $T_{solidus}$ and $T_{liquidus}$ above 30 GPa from this study, while the melting curve of Fe_7C_3 with 8.4 wt % carbon was slightly higher than the present $T_{liquidus}$ of the Fe-rich Fe-C system with 6.7 wt % carbon [*Lord et al.*, 2009]. Furthermore, the liquidus of the Fe-rich Fe-C system was extrapolated to inner core pressures using the Simon-Glatzel equation and agreed well with thermodynamic calculations [*Fei and Brosh*, 2014].

The addition of carbon and other light elements into iron can significantly affect the melting curve of iron at high pressures [*Li and Fei*, 2014]. The latest melting study of iron under static compression in a DAC up to 200 GPa by *Anzellini et al.* [2013], which also used diffuse scattering as a melting criteria and reached comparable *P-T* conditions, is used as the reference for comparing the carbon alloying effects on melting behavior of Fe-C system in this study. The solidus of Fe_3C is approximately 500 K lower than the melting point of Fe at 20–24 GPa [*Nakajima et al.*, 2009; *Fei and Brosh*, 2014]. The ΔT between the solidus of Fe_3C and the melting temperature of Fe gradually increases to approximately 1000 K at 145 GPa. On the other hand, iron carbide Fe_7C_3 exhibits a relatively higher melting temperature (liquidus) than Fe by ~300 K at 10–50 GPa [*Lord et al.*, 2009], different from other Fe-O, Fe-S, and Fe-Si alloys and compounds which largely depress the melting point of Fe [*Campbell et al.*, 2007; *Fischer and Campbell*, 2010; *Fischer et al.*, 2013]. The present $T_{liquidus}$ of the Fe-rich Fe-C system seems comparable to the melting curve of pure Fe below 90 GPa but is higher than that of pure Fe by ~500 K at 90–185 GPa [*Anzellini et al.*, 2013] (Figures 4 and S4).

Fe_7C_3 has been proposed to be a primary iron carbide phase in the inner core because of its phase stability, distinct elastic anisotropy, and extremely low shear wave velocities at relevant *P-T* conditions of the region [*Mookherjee et al.*, 2011; *Chen et al.*, 2014; *Wang et al.*, 2015]. Furthermore, *Fei and Brosh* [2014] theoretically predicted that Fe_3C could decompose into Fe_7C_3 and Fe between 136 and 330 GPa at core temperatures

based on thermodynamic calculations. This prediction determines the mineralogy of inner core if iron carbide is a stable phase in this region. Our experimental results here confirm the thermodynamic stability of Fe_7C_3 at conditions close to the Earth's inner core (Figure 1b). On the other hand, the presence of Fe_7C_3 in the inner core is debated due to the large uncertainty in the estimation of the eutectic carbon content in the molten Fe at core pressures and of the carbon concentration in the primitive liquid core [e.g., *Wood*, 1993; *Lord et al.*, 2009; *Wood et al.*, 2013; *Fei and Brosh*, 2014; *Nakajima et al.*, 2015; *Liu et al.*, 2016b] (Figure S4). Based on multiple approaches using carbon isotopes, mineral physics, the carbon/sulfur ratio, and sulfur content in the core [*Wood et al.*, 2013; *Nakajima et al.*, 2015], the carbon content of the Earth's core has been estimated to be 1.1 wt % as an upper bound. This upper bound value is much smaller than the calculated eutectic composition of the Fe-C system with 2.24 wt % carbon at the inner core boundary conditions [*Fei and Brosh*, 2014].

The relatively high melting point of Fe_7C_3 observed here may have implications for our understanding of the geophysics and geochemistry of the inner core. If the carbon content was on the carbon-rich side of the eutectic composition at the time of the inner core formation, Fe_7C_3 could crystallize as the first solid phase out of the molten core prior to hcp-Fe crystallizing in the region. Furthermore, iron carbide Fe_7C_3 has a comparable density to the present inner core [*Chen et al.*, 2014], indicating that the early-formed Fe_7C_3 could descend into the central part of the planet. Considering the density deficit of 3.6% at the inner-outer core boundary [*Fei et al.*, 2016], the Fe_7C_3 phase (containing ~8.4 wt % C) would not be abundant enough to constitute the whole inner core, indicating that the crystallizing process of Fe_7C_3 could have ended in the early stage of the formation of the inner core and that the carbon content in the present molten outer core is less than that of the eutectic composition of the Fe-rich Fe-C system at relevant Earth's core conditions. Consequently, Fe_7C_3 likely coexists with Fe in the inner part of the inner core, which may produce seismic anisotropy features that are distinct from the outer part of the inner core [*Ishii and Dziewoński*, 2002; *Wang et al.*, 2015]. Moreover, the presence of Fe_7C_3 in the inner core has a minimal effect on the total carbon content of the core as the volume of the innermost inner core, which is about 300–600 km in radius, is much less than 1% of the entire Earth's core. We note that there are large uncertainties on the total carbon content in the core and the eutectic composition of Fe-C system at Earth's core conditions. Further high *P-T* studies are thus needed in order to place tighter constraints on the stability of Fe_7C_3 and the eutectic composition of the Fe-rich Fe-C system at conditions relevant to Earth's core.

4. Conclusions

The phase relations and melting behavior of Fe_3C and Fe_7C_3 Fe-rich Fe-C system have been studied up to 185 GPa and 5200 K using X-ray diffraction measurements in a laser-heated DAC with the burst-heating technique. The diffuse scattering observed during laser heating was used as the primary indication for the presence of melt in the sample. The normalized intensity of diffuse signal from the liquid against temperature was fitted to derive the solidus and liquidus temperatures for the incongruent melting of the Fe-rich Fe-C system. We found that Fe_3C decomposes into a mixture of solid Fe_7C_3 and hcp-Fe above 145 GPa prior to melting and that Fe_7C_3 exhibits a relatively higher melting point than pure iron throughout relevant *P-T* conditions of the Earth's core. Our results indicated that Fe_7C_3 could crystallize out the molten core in early Earth and sink to the central part of the planet to be a constituent of the early solid inner core if the eutectic composition of the Fe-rich Fe-C system is less than the bulk carbon content of the core. Further experimental work is needed to assess the eutectic composition of the Fe-rich Fe-C system at *P-T* conditions of the inner core.

References

Anzellini, S., A. Dewaele, M. Mezouar, P. Loubeyre, and G. Morard (2013), Melting of iron at Earth's inner core boundary based on fast X-ray diffraction, *Science*, *340*(6131), 464–466, doi:10.1126/science.1233514.

Bazhanova, Z. G., A. R. Oganov, and O. Gianola (2012), Fe–C and Fe–H systems at pressures of the Earth's inner core, *Phys. Usp.*, *55*(5), 489–497, doi:10.3367/UFNr.0182.201205c.0521.

Boehler, R. (1993), Temperatures in the Earth's core from melting-point measurements of iron at high static pressures, *Nature*, *363*(6429), 534–536, doi:10.1038/363534a0.

Boehler, R., N. von Bargen, and A. Chopelas (1990), Melting, thermal expansion, and phase transitions of iron at high pressures, *J. Geophys. Res.*, *95*, 21,731–21,736, doi:10.1029/JB095iB13p21731.

Campbell, A. J. (2008), Measurement of temperature distributions across laser heated samples by multispectral imaging radiometry, *Rev. Sci. Instrum.*, *79*(1), 015108, doi:10.1063/1.2827513.

Campbell, A. J., C. T. Seagle, D. L. Heinz, G. Shen, and V. B. Prakapenka (2007), Partial melting in the iron–sulfur system at high pressure: A synchrotron X-ray diffraction study, *Phys. Earth Planet. Inter.*, *162*(1–2), 119–128, doi:10.1016/j.pepi.2007.04.001.

Chen, B., L. Gao, B. Lavina, P. Dera, E. E. Alp, J. Zhao, and J. Li (2012), Magneto-elastic coupling in compressed Fe$_7$C$_3$ supports carbon in Earth's inner core, *Geophys. Res. Lett.*, *39*, L18301, doi:10.1029/2012GL052875.

Chen, B., et al. (2014), Hidden carbon in Earth's inner core revealed by shear softening in dense Fe$_7$C$_3$, *Proc. Natl. Acad. Sci. U.S.A.*, *111*(50), 17,755–17,758, doi:10.1073/pnas.1411154111.

Dasgupta, R., A. Buono, G. Whelan, and D. Walker (2009), High-pressure melting relations in Fe–C–S systems: Implications for formation, evolution, and structure of metallic cores in planetary bodies, *Geochim. Cosmochim. Acta*, *73*(21), 6678–6691, doi:10.1016/j.gca.2009.08.001.

Dewaele, A., A. B. Belonoshko, G. Garbarino, F. Occelli, P. Bouvier, M. Hanfland, and M. Mezouar (2012), High-pressure–high-temperature equation of state of KCl and KBr, *Phys. Rev. B*, *85*(21), 214105, doi:10.1103/PhysRevB.85.214105.

Duman, E., M. Acet, E. F. Wassermann, J. P. Itié, F. Baudelet, O. Mathon, and S. Pascarelli (2005), Magnetic instabilities in Fe$_3$C cementite particles observed with Fe K-edge X-ray circular dichroism under pressure, *Phys. Rev. Lett.*, *94*(7), 075502, doi:10.1103/PhysRevLett.94.075502.

Fei, Y., and E. Brosh (2014), Experimental study and thermodynamic calculations of phase relations in the Fe–C system at high pressure, *Earth Planet. Sci. Lett.*, *408*, 155–162, doi:10.1016/j.epsl.2014.09.044.

Fei, Y., C. Murphy, Y. Shibazaki, A. Shahar, and H. Huang (2016), Thermal equation of state of hcp-iron: Constraint on the density deficit of Earth's solid inner core, *Geophys. Res. Lett.*, *43*, 6837–6843, doi:10.1002/2016GL069456.

Fischer, R. A., and A. J. Campbell (2010), High-pressure melting of wüstite, *Am. Mineral.*, *95*(10), 1473–1477, doi:10.2138/am.2010.3463.

Fischer, R. A., A. J. Campbell, D. M. Reaman, N. A. Miller, D. L. Heinz, P. Dera, and V. B. Prakapenka (2013), Phase relations in the Fe–FeSi system at high pressures and temperatures, *Earth Planet. Sci. Lett.*, *373*, 54–64, doi:10.1016/j.epsl.2013.04.035.

Gao, L., et al. (2008), Pressure-induced magnetic transition and sound velocities of Fe$_3$C: Implications for carbon in the Earth's inner core, *Geophys. Res. Lett.*, *35*, L17306, doi:10.1029/2008GL034817.

Ishii, M., and A. M. Dziewoński (2002), The innermost inner core of the earth: Evidence for a change in anisotropic behavior at the radius of about 300 km, *Proc. Natl. Acad. Sci. U.S.A.*, *99*(22), 14,026–14,030, doi:10.1073/pnas.172508499.

Larson, A. C., and R. B. V. Dreele (1994), General Structure Analysis System (GSAS), Los Alamos National Laboratory Report LAUR 86–748.

Li, J., and Y. Fei (2014), Experimental constraints on core composition, in *Treatise on Geochemistry (2nd Edition)*, edited by H. D. Holland and K. K. Turekian, pp. 527–557, Elsevier, Oxford.

Li, J., H. K. Mao, Y. Fei, E. Gregoryanz, M. Eremets, and C. S. Zha (2002), Compression of Fe3C to 30 GPa at room temperature, *Phys. Chem. Miner.*, *29*(3), 166–169, doi:10.1007/s00269-001-0224-4.

Lin, J.-F., V. V. Struzhkin, H.-k. Mao, R. J. Hemley, P. Chow, M. Y. Hu, and J. Li (2004), Magnetic transition in compressed Fe$_3$C from X-ray emission spectroscopy, *Phys. Rev. B*, *70*(21), 212405, doi:10.1103/PhysRevB.70.212405.

Litasov, K. D., I. S. Sharygin, P. I. Dorogokupets, A. Shatskiy, P. N. Gavryushkin, T. S. Sokolova, E. Ohtani, J. Li, and K. Funakoshi (2013), Thermal equation of state and thermodynamic properties of iron carbide Fe$_3$C to 31 GPa and 1473 K, *J. Geophys. Res. Solid Earth*, *118*, 5274–5284, doi:10.1002/2013JB010270.

Liu, J., J. Li, and D. Ikuta (2016a), Elastic softening in Fe7C3 with implications for Earth's deep carbon reservoirs, *J. Geophys. Res. Solid Earth*, *121*, 1514–1524, doi:10.1002/2015JB012701.

Liu, J., J. Li, R. Hrubiak, and J. S. Smith (2016b), Origins of ultra-low velocity zones through slab-derived metallic melt, *Proc. Natl. Acad. Sci. U.S.A.*, *113*(20), 5547–5551, doi:10.1073/pnas.1519540113.

Lord, O. T., M. J. Walter, R. Dasgupta, D. Walker, and S. M. Clark (2009), Melting in the Fe–C system to 70 GPa, *Earth Planet. Sci. Lett.*, *284*(1–2), 157–167, doi:10.1016/j.epsl.2009.04.017.

Mookherjee, M., Y. Nakajima, G. Steinle-Neumann, K. Glazyrin, X. Wu, L. Dubrovinsky, C. McCammon, and A. Chumakov (2011), High-pressure behavior of iron carbide (Fe$_7$C$_3$) at inner core conditions, *J. Geophys. Res.*, *116*, B04201, doi:10.1029/2010JB007819.

Nakajima, Y., E. Takahashi, T. Suzuki, and K.-i. Funakoshi (2009), "Carbon in the core" revisited, *Phys. Earth Planet. Inter.*, *174*(1–4), 202–211, doi:10.1016/j.pepi.2008.05.014.

Nakajima, Y., E. Takahashi, N. Sata, Y. Nishihara, K. Hirose, K.-i. Funakoshi, and Y. Ohishi (2011), Thermoelastic property and high-pressure stability of Fe7C3: Implication for iron-carbide in the Earth's core, *Am. Mineral.*, *96*(7), 1158–1165, doi:10.2138/am.2011.3703.

Nakajima, Y., S. Imada, K. Hirose, T. Komabayashi, H. Ozawa, S. Tateno, S. Tsutsui, Y. Kuwayama, and A. Q. R. Baron (2015), Carbon-depleted outer core revealed by sound velocity measurements of liquid iron-carbon alloy, *Nat. Commun.*, *6*, 8942, doi:10.1038/ncomms9942.

Prakapenka, V. B., A. Kubo, A. Kuznetsov, A. Laskin, O. Shkurikhin, P. Dera, M. L. Rivers, and S. R. Sutton (2008), Advanced flat top laser heating system for high pressure research at GSECARS: Application to the melting behavior of germanium, *High Pressure Res.*, *28*(3), 225–235, doi:10.1080/08957950802050718.

Prescher, C., and V. B. Prakapenka (2015), DIOPTAS: A program for reduction of two-dimensional X-ray diffraction data and data exploration, *High Pressure Res.*, *35*(3), 223–230, doi:10.1080/08957959.2015.1059835.

Prescher, C., L. Dubrovinsky, C. McCammon, K. Glazyrin, Y. Nakajima, A. Kantor, M. Merlini, and M. Hanfland (2012), Structurally hidden magnetic transitions in Fe3C at high pressures, *Phys. Rev. B*, *85*(14), 140402, doi:10.1103/PhysRevB.85.140402.

Prescher, C., et al. (2015), High Poisson's ratio of Earth's inner core explained by carbon alloying, *Nat. Geosci.*, *8*, 220–223, doi:10.1038/ngeo2370.

Sata, N., K. Hirose, G. Shen, Y. Nakajima, Y. Ohishi, and N. Hirao (2010), Compression of FeSi, Fe3C, Fe$_{0.95}$O, and FeS under the core pressures and implication for light element in the Earth's core, *J. Geophys. Res.*, *115*, B09204, doi:10.1029/2009JB006975.

Scott, H. P., Q. Williams, and E. Knittle (2001), Stability and equation of state of Fe3C to 73 GPa: Implications for carbon in the Earth's core, *Geophys. Res. Lett.*, *28*, 1875–1878, doi:10.1029/2000GL012606.

Shen, G., V. B. Prakapenka, M. L. Rivers, and S. R. Sutton (2004), Structure of liquid iron at pressures up to 58 GPa, *Phys. Rev. Lett.*, *92*(18), 185701, doi:10.1103/PhysRevLett.92.185701.

Simon, F., and G. Glatzel (1929), Remarks on fusion pressure curve, *Z. Anorg. Allg. Chem.*, *178*(1), 309–316, doi:10.1002/zaac.19291780123.

Tateno, S., K. Hirose, Y. Ohishi, and Y. Tatsumi (2010), The structure of iron in Earth's inner core, *Science*, *330*(6002), 359–361, doi:10.1126/science.1194662.

Toby, B. (2001), EXPGUI, a graphical user interface for GSAS, *J. Appl. Cryst.*, *34*(2), 210–213, doi:10.1107/S0021889801002242.

Wang, T., X. Song, and H. H. Xia (2015), Equatorial anisotropy in the inner part of Earth's inner core from autocorrelation of earthquake coda, *Nat. Geosci.*, *8*(3), 224–227, doi:10.1038/ngeo2354.

Williams, Q., R. Jeanloz, J. Bass, B. Svendsen, and T. J. Ahrens (1987), The melting curve of iron to 250 Gigapascals: A constraint on the temperature at Earth's center, *Science*, *236*(4798), 181–182, doi:10.1126/science.236.4798.181.

Wood, B. J. (1993), Carbon in the core, *Earth Planet. Sci. Lett.*, *117*(3–4), 593–607, doi:10.1016/0012-821X(93)90105-I.

Wood, B. J., J. Li, and A. Shahar (2013), Carbon in the core: Its influence on the properties of core and mantle, *Rev. Mineral. Geochem.*, *75*(1), 231–250, doi:10.2138/rmg.2013.75.8.